Investigation of flying height stability of thermal fly-height control sliders in lubricant or solid disk contact with roughness

Jinglin Zheng and David B. Bogy

Computer Mechanics Laboratory

Department of Mechanical Engineering

University of California

Berkeley, CA 94720

Abstract

When the magnetic spacing in hard disk drives is reduced to sub-3nm, contact between the slider and disk becomes inevitable. Stability analysis is used in this study to investigate the head-disk interface (HDI) stability of thermal fly-height control (TFC) sliders in light contact with the disk lubricant or solid roughness. We implement an improved DMT model with sub-boundary lubrication into the CML air bearing program and analyze the stability of equilibrium states of a TFC slider under different thermal actuations. It is found that stability is lost when the slider penetrates deeper into the lubricant layer, due to a fast growth in the adhesion force, and it is restored when the solid roughness contact develops. In addition, the critical point for the onset of this instability and the range of this instability region is found to vary with lubricant thickness and protrusion surface steepness, while keeping the TFC design the same.

Keywords

TFC slider, instability, interfacial adhesion, head-disk interface

Introduction

To push the areal density in magnetic recording hard disk drives to 5-10 terabits per square inch, the magnetic spacing between the slider and disk should be reduced to sub-3 nanometers. Excluding the thickness of the DLC overcoats on both slider and disk (~1nm), the surface roughness (~0.75nm) and the lubricant thickness (~1nm), the possible physical spacing or flying clearance is reduced to only ~0.25nm. At such a small physical spacing, the slider's contact with the disk, or at least with the lubricant layer becomes inevitable.

One promising scheme for such an ultra-high density recording is to allow have a part of the slider at the read/write transducer area be in contact with the lubricant layer while most of the slider remains well above the disk, being supported by the air bearing. In [1], a so-called lubricant-surfing recording scheme was proposed where the current TFC technology is utilized to produce a protruded part on the air bearing surface. When actuated, this protruded part can penetrate into the lubricant layer during reading or writing. This method potentially has the advantage of reducing the physical spacing while avoiding solid slider-disk contact. A major concern associated with this approach is that at the near-contact region, the HDI stability might be compromised by the increasingly significant interfacial forces. The investigations in [1-2] modeled the lubricant as a soft solid layer that is plastically deformed under contact. A power law was adopted for calculating the contact force. However, for the intermolecular adhesion, the deformation profile of the contact area was not considered in [1-2]. It was shown through dynamic simulations that a lubricant-surfing status could be reached within certain protrusion height limits.

In this study, we apply a stability analysis to a TFC slider in contact with a disk lubricant and possibly also roughness. By adopting a sub-boundary lubrication model [3] based on the classical DMT model, we include the effects of lubricant-contacting and solid-contacting adhesion where the deformed contact profile is taken into account. The real TFC protrusion profile is applied for an industry produced, femto-sized slider (0.85×0.70×0.23mm). The equilibrium solution is examined as a function of the thermal protrusion. An instability region is found as the slider comes

into contact with the lubricant layer or the solid disk roughness. The effects of lubricant thickness and protrusion profile on the range of the instability region and the critical point for the onset of instability are also investigated.

Adhesion and contact models

To consider the effect of contact with the lubricant/disk roughness, asperity-based adhesion models are needed. In addition, the presence of a monolayer of lubricant must be considered as it makes a large contribution to the interfacial adhesion at extremely small HDI clearances. Here we adopt the sub-boundary lubrication model proposed by Stanley et al [3], which is based primarily on the improved DMT model. As both the slider and disk surfaces are covered with DLC overcoats, the DMT model is more suitable for modeling the contact between these two solid surfaces. Furthermore, the existence of a lubricant layer and its thickness are also taken into account in this model. The total adhesion force F_s is given by [3]:

$$\begin{aligned} F_s = \eta A_n \Big(& \int_{-\infty}^{d-t} \frac{8}{3}\pi R\delta\gamma\left[\left(\frac{\varepsilon}{d-u-t+\varepsilon}\right)^2 - 0.25\left(\frac{\varepsilon}{d-u-t+\varepsilon}\right)^8\right]\phi(u)du \\ & + 2\pi R\delta\gamma \int_{d-t}^{d} \phi(u)du \\ & + \int_{d}^{\infty}\int_{r_t}^{\infty} \frac{8}{3}\frac{\delta\gamma}{\varepsilon}\left[\left(\frac{\varepsilon}{z-t+\varepsilon}\right)^3 - \left(\frac{\varepsilon}{z-t+\varepsilon}\right)^9\right]\cdot 2\pi r dr\phi(u)du\Big) \end{aligned} \tag{1}$$

where η is the areal density of asperities, A_n is the nominal contact area, R is the asperity radius, $\delta\gamma$ is the adhesion energy per unit area, ε is the equilibrium intermolecular distance, d is the separation of the mean plane of asperity heights, u is the asperity height, t is the thickness of the lubricant layer, $\Phi(u)$ is the asperity height distribution function. Fig. 1 is a schematic diagram illustrating the parameters involved in equation (1).

In the third integral in equation (1), z is the separation of solid surfaces outside the contact region at a radius r, and r_t is the radius at the intersection of the lubricant and solid, as shown in Fig. 2.

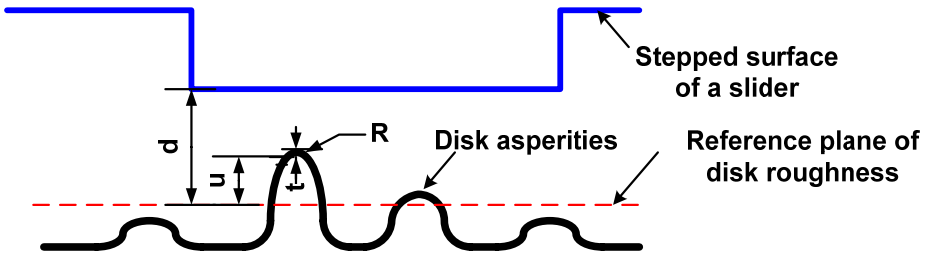

Fig. 1 Schematic diagram of slider and disk surfaces not in contact

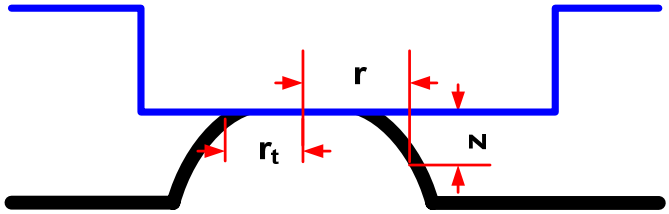

Fig. 2 Schematic diagram of an asperity in solid contact with a plane

The first integral in equation (1) gives the adhesion force arising from non-contacting asperities. It is the integration of the attractive pressure derived from the Lennard-Jones potential over a sphere-shaped profile [4]. The second integral is the contribution of the lubricant-contacting asperities. The third integral comes from the solid-contacting asperities. We only consider elastic contact here. For the third integral, the separation z of solid surfaces at a radius r is given by [4]:

$$z = \frac{1}{\pi R}[a(r^2 - a^2)^{1/2} - (2a^2 - r^2)\tan^{-1}(\frac{r^2}{a^2} - 1)^{1/2}] \tag{2}$$

where $a=(\omega R)^{1/2}$ is the radius of the contact region, $\omega=u-d$ is the interference.

Several multi-asperity contact models have been developed giving different relationships between the contact pressure and the separation of two parallel rough surfaces. Chen and Bogy showed that the GW model, CEB model and KE model give similar results provided that the plasticity index of the contact interface is small and only a few of the contacting asperities are fully plastically deformed [5]. Here we use the GW model which gives the contact pressure P as [6]:

$$P = \frac{4}{3}\eta A_n E R^{1/2} \int_d^{\infty} (u-d)^{3/2} \phi(u) du \tag{3}$$

where E is the combined elastic modulus of the two surfaces. Note that by adopting this interfacial force model, the contact force is not affected by the lubricant thickness t.

Several assumptions are associated with the above interfacial force model: the lubricant is uniformly distributed on the disk roughness and is mobile, the thickness of the lubricant layer is constant since only a small portion of lubricant is displaced under contact with the protruded slider. We also restrict the asperity deformation to be elastic. No bulk deformation and asperity interaction occurs. Since only a small protruded part of the slider comes into contact, we also neglect the pressure loss in the air bearing in contact.

Static simulation of a TFC slider

The CMLair static simulation program is used to perform the FH stability investigation. This program uses a Quasi-Newton iteration method to search for an equilibrium flying state of a slider. The Fukui-Kaneko slip correction is adopted in this program to modify the generalized Reynolds equation to account for the rarefaction effects in the air bearing. Patankar's control volume method is applied to discretize the modified Reynolds equation. The equation is then solved using an alternating direction line sweeping method [7]. In the implementation of the interfacial force model, each grid in the air bearing surface is regarded as a flat and smooth surface. Combined roughness parameters are applied on the disk. The asperity height distribution function $\Phi(u)$ is assumed to be a normal distribution with a mean of 0 and a standard deviation σ. The integrated interfacial force and torques (including adhesion, contact and friction forces) is balanced by the air bearing pressure and the suspension load for an equilibrium solution.

The effects of TFC protrusion are taken into account by modifying the profile of the ABS, thereby changing the separation between the slider and the disk. For simplicity, we adopt the protrusion profile in Fig. 3 as a base profile and modify this profile proportionally to achieve a higher or lower protrusion profile. The base profile is obtained by using the CML TFC program which solves the equilibrium flying

attitude and deformation of a TFC slider through an iterative approach [8, 9, 12]. Table 1 gives the roughness and protrusion parameters involved in the simulations.

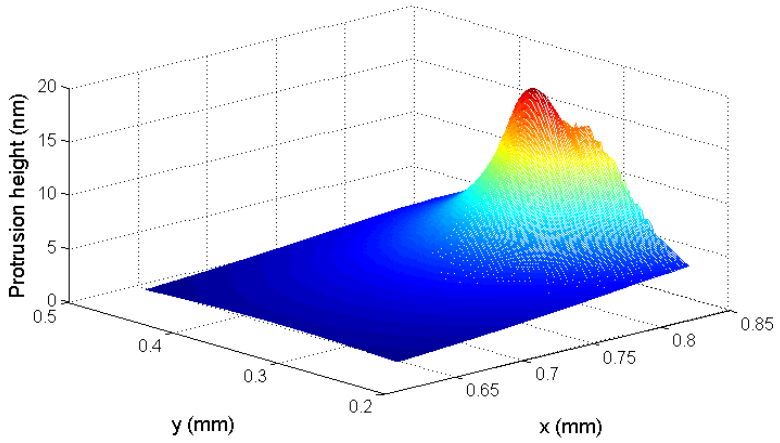

Fig. 3 Thermal protrusion profile obtained through an iterative approach

Table 1 Simulation parameters [5, 10]

Mean radius of asperities R (μm)	6.384
Asperity density η ($1/m^2$)	9.871×10^{12}
Standard deviation of asperity heights σ (nm)	0.654
Equilibrium intermolecular distance ε (nm)	0.3
Combined elastic modulus (GPa)	111.59
Friction coefficient	0.2
Adhesion energy per unit area $\delta\gamma$ (N/m)	0.151
Protrusion area (mm)	0.21×0.24
Peak thermal protrusion height for the base profile TP^* (nm)	17.2927
Lubricant thickness t(nm)	0.8, 1.0, 1.2

Results and discussion

Existence of an instability region

Fig. 4 shows the variation of the minimum separation d^* between the slider and disk for different thermal protrusion amounts and for lubricant thickness t=1.0nm. Each data point in Fig. 4 represents an equilibrium flying-state obtained by the

CMLair static solver. A dot means a positive stiffness is associated with this flying-state, while a star designates a negative stiffness. As seen in the figure, a region of negative stiffness extends from d^*=1.39 to d^*=0.35, accompanied with a steeper decrease in d^*.

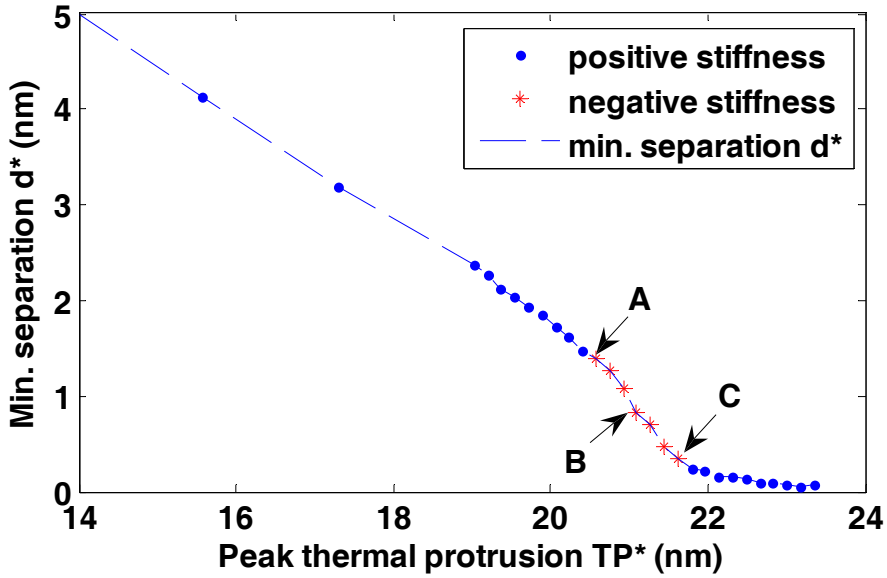

Fig. 4 Minimum separation d^* at equilibrium for different thermal protrusions Points with negative stiffness are marked out with stars. Points A, B, C mark the onset, middle and ending of the instability region, the equilibrium states of which will be further analyzed below.

Fig. 5 shows the variation of total interfacial force and adhesion force with increasing thermal protrusion. The instability points are marked with stars on the adhesion force curve. In the range of instability, a rapid increase in the magnitude of adhesion force with increased protrusion is seen. It is apparent that this rapid increase in the adhesion force magnitude at this region is related to the onset of HDI instability. In addition, the curve for total interfacial force is almost overlapped with the adhesion force curve until the end of the instability region where the interfacial force curve branches from the adhesion force. The difference between these two curves equals to the magnitude of the contact force at the slider-disk interface which is shown in Fig. 6. The rapid increase in the contact force with protrusion in this region explains the restoration of HDI stability.

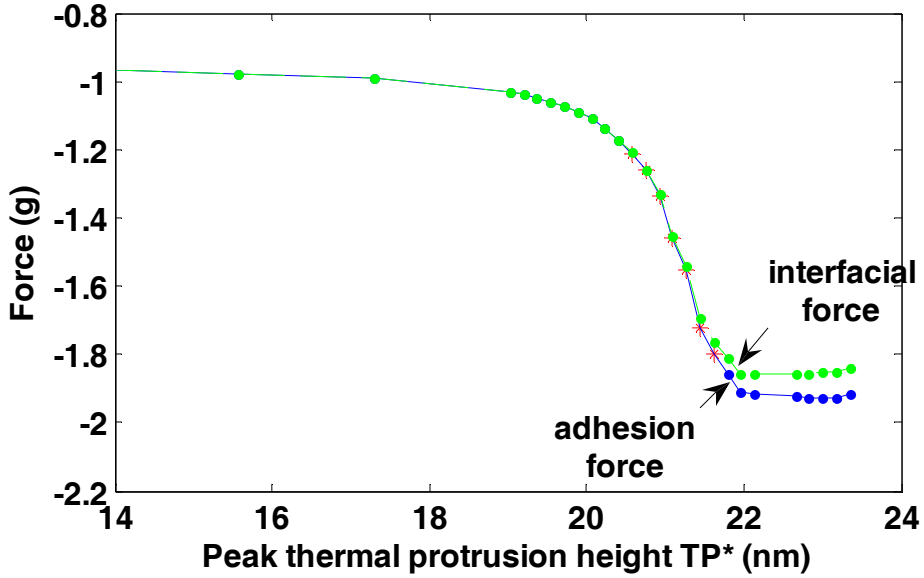

Fig. 5 Interfacial forces at equilibrium for different thermal protrusions
Points with negative stiffness marked out with stars.

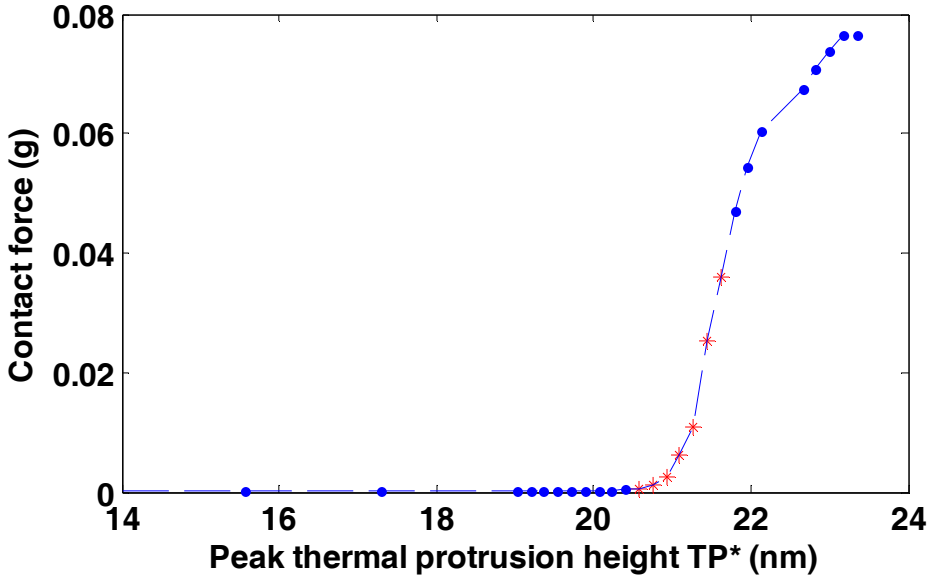

Fig. 6 Interfacial contact force at equilibrium for different thermal protrusions.
Points with negative stiffness are marked with stars.

The sign of the system stiffness is derived from the stiffness matrix which is defined by the following 3×3 matrix:

$$\begin{bmatrix} \partial F/\partial z & \partial F/\partial \theta & \partial F/\partial \varphi \\ \partial T_\theta/\partial z & \partial T_\theta/\partial \theta & \partial T_\theta/\partial \varphi \\ \partial T_\varphi/\partial z & \partial T_\varphi/\partial \theta & \partial T_\varphi/\partial \varphi \end{bmatrix}$$

where z represents the flying-height coordinate, θ is the pitch angle, φ is the roll angle,

F is the total force in the flying-height direction, T_θ is the total pitch torque, and T_φ is the total roll torque. If all three eigenvalues of the stiffness matrix are positive, the system has a positive stiffness. Otherwise, the system stiffness is negative [11].

Next we consider point A of Fig. 4, which is located at the beginning of the instability region, and calculate the total force acting on the slider under small disturbances of the flying-height (±2% disturbances). The result is shown in Fig. 7(a), Note that the sign convention here is that an upward force has a positive sign and a downward one has a negative sign. As seen from Fig. 7(a), an upward disturbance in flying-height results in a downward force which pulls the slider back to the equilibrium state A. However, a downward disturbance in flying-height results in a negative total force which pulls the slider further towards the disk. The slope of the total force curve is determined by the rate of change in the air bearing force and interfacial force with respect to z (as the suspension load remains constant). Instability under a downward disturbance at state A means the growth in interfacial adhesion due to a flying-height drop overwhelms the increase in the air bearing lift at this point, which causes the loss of HDI stability.

Similarly, at state B of Fig. 4, a downward disturbance leads to a negative force further pulling the slider into contact with the disk, and an upward disturbance results in a positive force further pushing the slider away from the disk, as shown in Fig. 7(b). For state C of Fig. 4, while a downward disturbance results in a positive force pushing the slider back to state C, an upward disturbance leads to a positive force further pushing the slider to fly higher, as shown in Fig. 7(c). Thus, in the star-marked region, any flying-height disturbance results in either a higher slider flying-height, or deeper contact between the slider and disk.

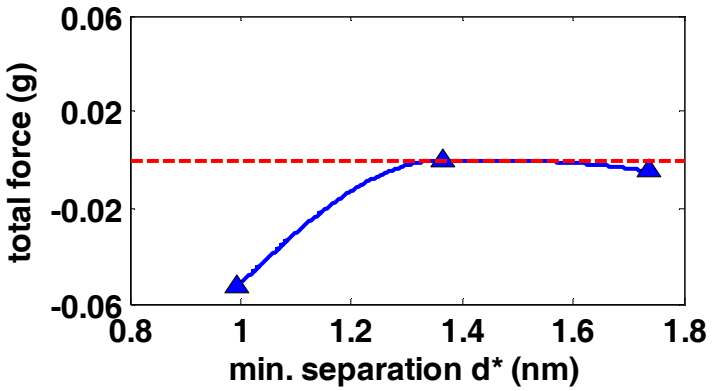

(a) instability for point A

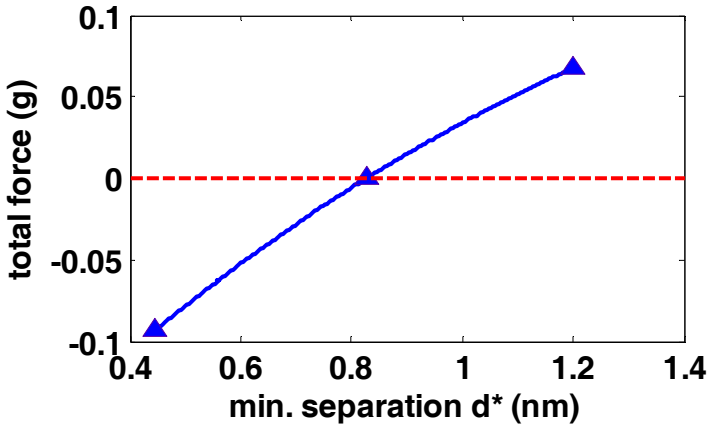

(b) Instability for point B

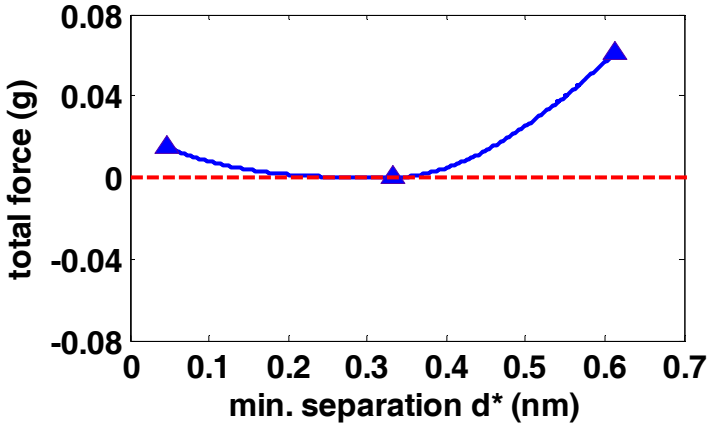

(c) Instability for point C

Fig. 7 Instability of the equilibrium states A, B, and C under flying-height disturbances

Fig. 8 shows the interfacial adhesion force dependence on the head-disk separation. The three contributions to the adhesion force (i.e., the three integrals in equation (1)) are also plotted. Here we mark the minimum head-disk separation at

point A and point C on Fig. 6 by the two vertical dashed lines. h_A is not exactly at the location where the lubricant-contact force begins to reduce steeply with decreasing h. Instead, it is shifted to the left, which means that at this point, a part of the protruded slider is in contact with the lubricant layer. Furthermore, h_c is shifted to the left of the point where the solid-contact adhesion force begins to decrease rapidly with decreasing spacing, which means that at this point, the slider enters into partial contact with the disk.

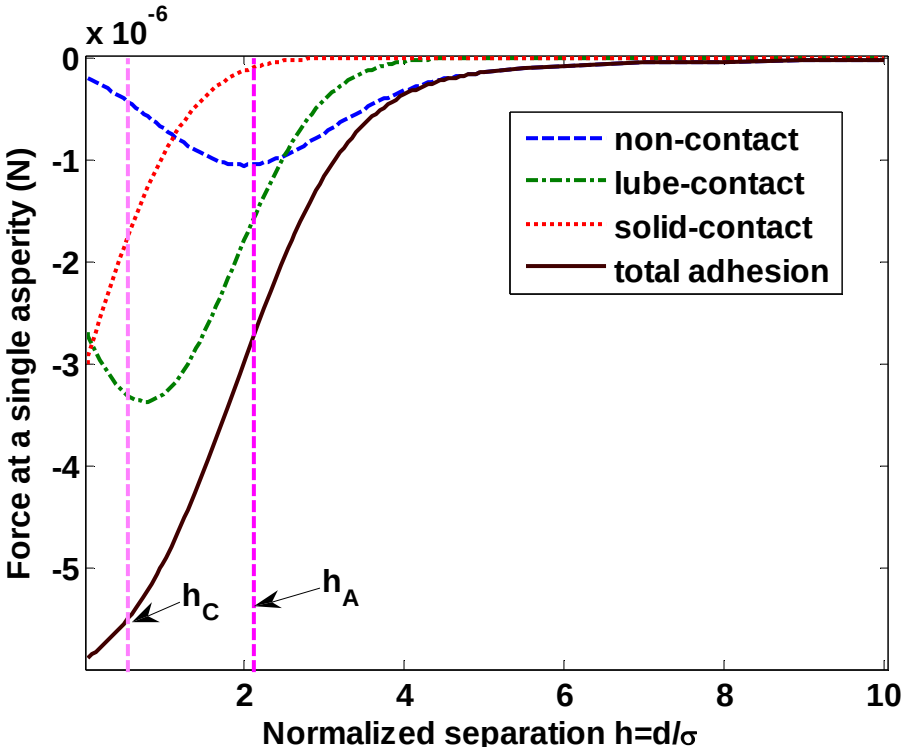

Fig. 8 Interfacial adhesion at different slider-disk separations
The minimum separations for states A and C are marked with h_A and h_C

In Fig. 9, we take a closer look at the increase in adhesion force magnitude near the instability region. We plot the contributions from non-contact, lubricant-contact and solid-contact adhesion on the same scale. It is obvious that the lubricant-contact force accounts for the largest part of the increase in interfacial adhesion, which means a larger portion of the protruding part is coming into contact with the lubricant at the instability region.

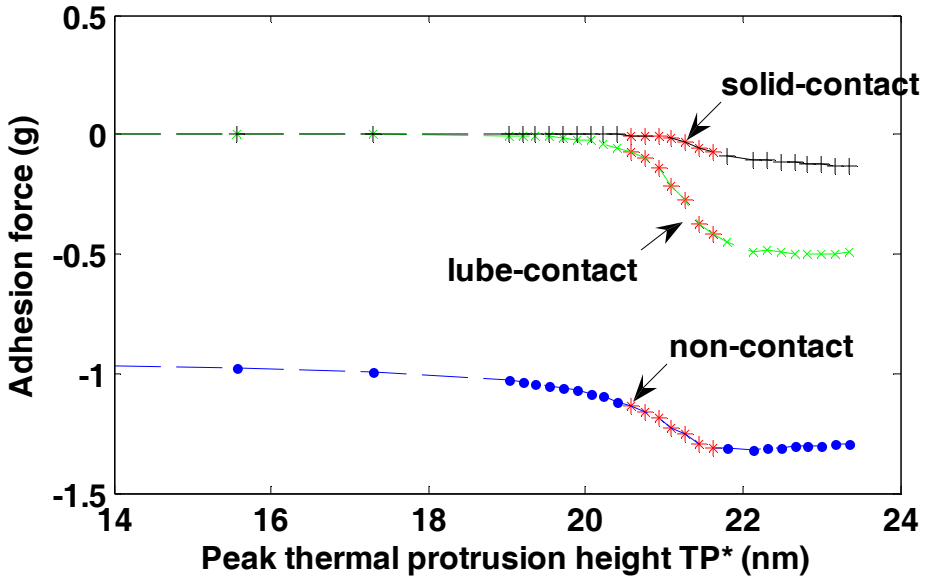

Fig. 9 Components of interfacial adhesion at equilibrium for different thermal protrusions. Negative stiffness points are marked with stars.

Effect of lubricant thickness

Since we have found that the fast growth in interfacial adhesion is associated with the HDI instability found in simulations, different lubricant thicknesses may affect the range of the instability region as t is related to the adhesion force according to equation (1). Here we investigate three lubricant thicknesses t=0.8, 1.0 and 1.2nm with the same roughness parameters and protrusion profile. The relationships between the minimum slider-disk separation d^* and the thermal protrusion amount TP^* for the three cases are shown in Fig. 10. To compare the instability regions of the three cases, we mark the negative stiffness state with stars. As shown in Fig. 10, at the same peak thermal protrusion (the ABS is exactly the same), the stiffness of the HDI drops with increasing lubricant thickness (d^* drops with increasing lubricant thickness). Also, the critical TP^* (TP^* at the starting point of the instability region) is 21.27nm, 20.58nm and 19.89nm for t=0.8, 1.0 and 1.2nm, respectively. Therefore with a thinner lubricant layer, we are allowed to actuate the slider to a higher protrusion while maintaining a stable HDI. The corresponding critical d^* for t=0.8nm is 1.18 nm, the lowest among the three, which means that in this case the slider can get closest to the disk, without losing the HDI stability or getting into severe contact with the disk. This result also shows that although it seems that in a lube-surfing recording scheme, we

may even relax the limit on lubricant thickness to some extent [1], as the slider is allowed to make contact with the lubricant, a thicker lubricant can result in a less stable HDI: the slider is not able to maintain a stable, ultra-low flying-height and is pushed back to a high flying-state or gets into solid contact with the disk roughness.

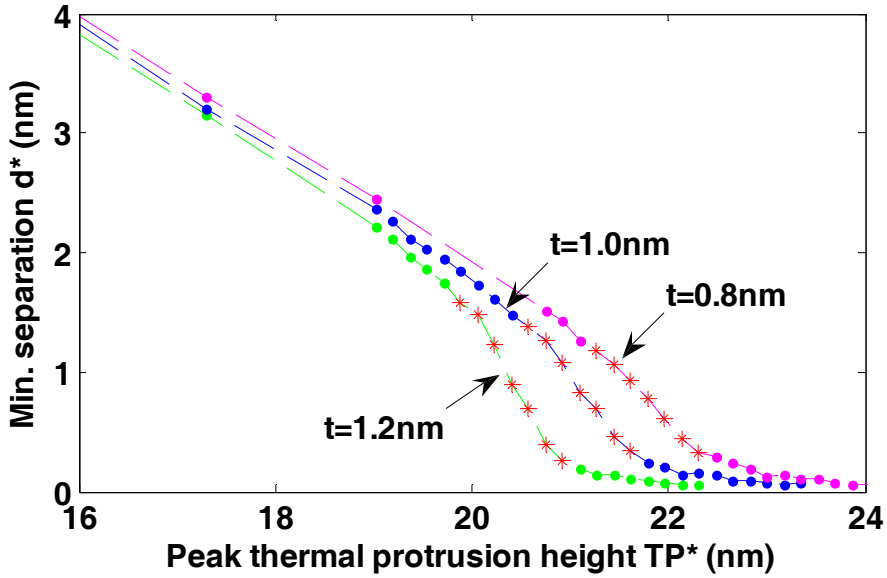

Fig. 10 Minimum separation *d** at equilibrium at different thermal protrusions for t=0.8nm, 1.0nm and 1.2nm

Effect of protrusion profile

The profile of thermal protrusion is another factor that can be associated with the effects of interfacial forces. Consider the three protrusion profiles shown in Fig. 11, which are viewed from the trailing edge of the slider and pass through the point with the peak protrusion height. The middle solid curve, which is calculated using the CML TFC program, is taken as a base profile, and is denoted as case B. By increasing or decreasing the base area of case B, we get a steepened profile, case I, or a flattened profile, case J, with the same peak protrusion height. If the slider is fixed at zero pitch and roll, and moves toward the disk, we can expect that the case with the steepest profile should be less affected by the fast-increasing interfacial adhesion since a smaller part of the protrusion is in closer contact with the disk.

Here we take *t*=1.0nm and calculate the instability regions for cases B, I and J respectively. The thermal actuation for each case is modified by increasing the protrusion height proportionally with respect to the original profiles shown in Fig. 11.

Interestingly, the result is not monotonic with respect to the steepness of the protrusion profiles. The critical d^* marking the onset of instability in case I, instead of being lower due to the steepened protrusion, is 1.55nm, i.e., higher compared with 1.39nm of case B. For a specific TP^*, which means we are keeping peak protrusion height the same for both cases, case I gives a lower flying-height, even when the interfacial forces are negligible (according to Fig. 6, the interfacial adhesion takes effect at d=5nm). This shows that for the same TP^*, the air bearing is less stiff in case I. since the critical d^* is determined by the rate of change in both the air bearing forces and interfacial forces, the stiffness of the air bearing in case I fails to balance the fast growth in adhesion and results in an earlier onset of instability.

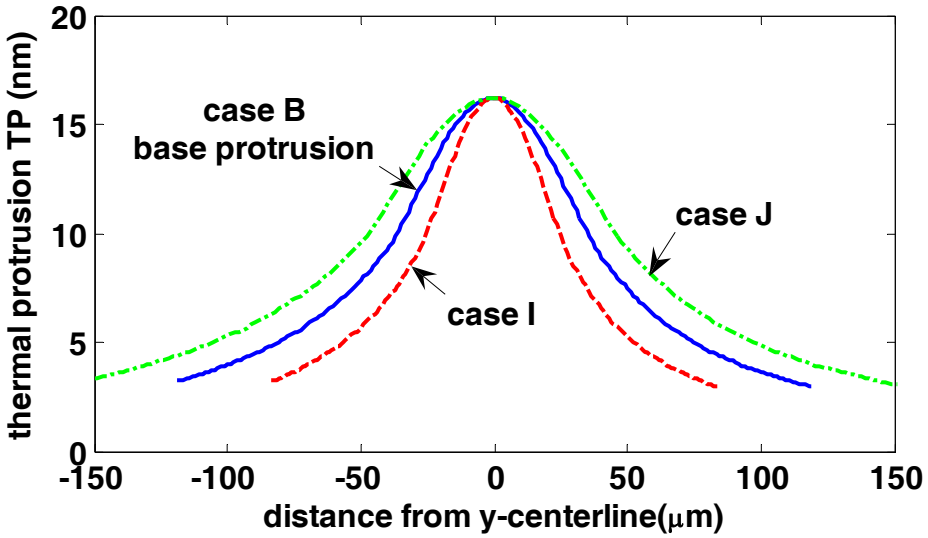

Fig. 11 Protrusion profiles with different base areas

In comparison, case J, which has the flattened profile, enters the instability region at d^*=1.53nm, almost the same as case I. As shown in Fig. 12, case J has a stiffer air bearing, shown by the highest flying-height among the three when the interfacial forces are negligible. The stiffness of the air bearing compensates the faster increase in the adhesion force in case J, and keeps the critical d^* almost unchanged compared with case I. Therefore, although the steeper protrusion may be preferred in the sense that the slider is less sensitive to the growing interfacial force as it moves toward the disk, this may trade off with a less stiff air-bearing which, in turn, reduces the HDI stability, as shown by case I. Among the three cases, case B provides a protrusion

profile less sensitive to interfacial forces while maintaining sufficient air bearing stiffness. This demonstrates that through optimization of the TFC heater design, it is possible to achieve a lower critical d^*, or a wider range for stable lube-surfing recording.

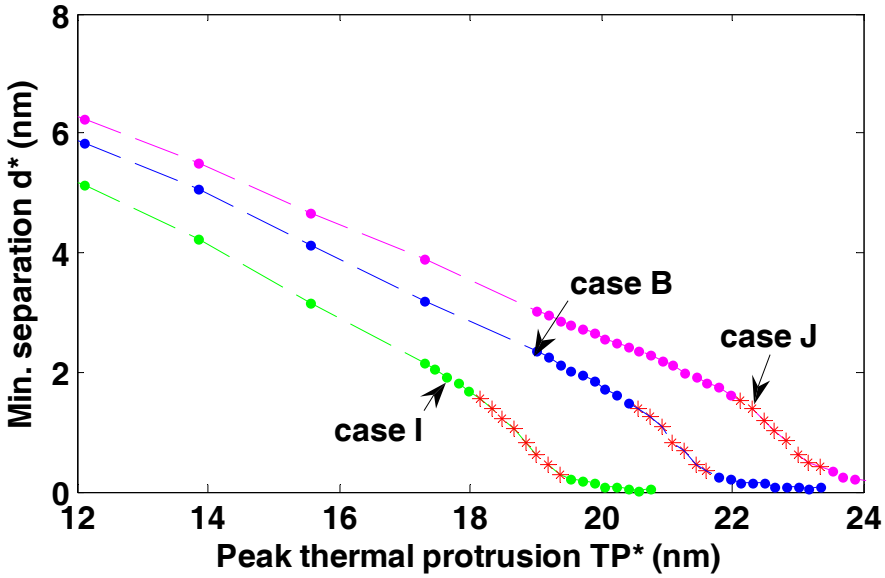

Fig. 12 Minimum separation d^* at equilibrium of different thermal protrusions for cases B (base profile), I (steepened profile), J (flattened profile)

Conclusion

By including interfacial force models considering the effects of boundary-lubrication, we find an instability region exists as a TFC slider comes into contact the disk lubricant or the disk surface roughness through increased thermal protrusions: the slider maintains a stable equilibrium state in light contact with the lubricant; but stability is lost when the contact gets more severe; and the stability returns as the slider enters deep-contact with the disk roughness. Existence of such an instability region is related to a fast growth of interfacial adhesion which is not balanced by the rate of change in the air bearing lift. This growth in interfacial adhesion is mainly caused by the lubricant-contacting adhesion.

The effects of lubricant thickness and protrusion steepness on this instability region are investigated. A thinner lubricant layer is beneficial for narrowing the extent of this region and reducing the critical spacing beyond which instability occurs. As for the protrusion steepness, although less sensitivity to the increased interfacial

adhesion is expected for a steeper protrusion, this may trade off with a less stiff air bearing. Thus, optimization in TFC design is necessary for achieving the largest possible stability region in the lubricant-contact recording scheme.

Reference

1. Liu, B., Zhang, M. S., Yu, S. K., Hua, W., Ma, Y. S., Zhou, W. D., Gonzaga, L., Man, Y. J., 2009, "Lubricant-surfing Recording and Its Feasibility Exploration," *IEEE Trans. Magn.*, **45**(2), pp. 899-904
2. Hua, W., Liu, B., Yu, S., Zhou, W., 2009, "Nanoscale roughness contact in a slider-disk interface," *Nanotechnology*, **20** (285710)
3. Stanley, H. M., Etsion I., Bogy, D. B., 1990, "Adhesion of Contacting Rough Surfaces in the Presence of Sub-Boundary Lubrication," *Transactions of the ASME*, Vol. 112, pp. 98-104
4. Muller, V. M., Derjaguin, B.V., Toporov, Yu. P., 1983, "On Two Methods of Calculation of the Force of Sticking of an Elastic Sphere to a Rigid Plane," *Colloids and Surfaces*, vol. 7, pp. 251-259
5. Chen, D., Bogy, D. B., 2007, "Intermolecular Force and Surface Roughness Models for Air Bearing Simulations for Sub-5nm Flying Height Sliders," *Microsystem Technologies,* vol. 13, pp. 1211-1217
6. Greenwood, J. A., Williamson, J. B. P., 1966, "Contact of Nominally Flat surfaces," *Proceedings of the Royal Society of London, Series A, Mathematical and Physical Sciences*, **112**(1442), pp. 300-319
7. Lu, S., 1997, "Numerical Simulation of Slider Air Bearings, ", Doctoral Dissertation
8. Juang, J., Chen, D., Bogy, D.B., 2006, "Alternate air bearing slider design areal density of 1 Tb/in^2," *IEEE Trans. Magn.*, **42**(2), pp. 241-246
9. Zheng, J., Bogy, D. B., 2009, "Thermal Fly-Height Control (TFC) code user's manual", *CML Blue Report,* 2009-06
10. Suh, A. Y., Polycarpou, A. A., 2005, "Dynamic Adhesive Instability of Sub-Five Nanometer Head-Disk Interfaces," *Proceedings of the 13th Mediterranean*

Conference on Control and Automation, pp. 139-146

11. Gupta, V., Bogy, D. B., 2005, "Dynamics of Sub-5nm Air Bearing Sliders in the Presence of Electrostatic and Intermolecular Forces at the Head Disk Interface", *IEEE Trans. Magn.*, **41**(2), pp. 610-615
12. J. Zheng, D. B. Bogy, S. Zhang, W. Yan, 2009, "Effects of altitude on the thermal flying height actuation", *Proceedings of the ASME/STLE International Joint Tribology Conference (2009)*